

Nonlinear bound states in the continuum of a one-dimensional photonic crystal slabS. D. Krasikov,^{*} A. A. Bogdanov, and I. V. Iorsh
ITMO University, Saint Petersburg 197101, Russia

(Received 27 March 2018; published 25 June 2018)

The optical bound state in the continuum (BIC) is characterized by an extremely high-quality factor resulting in a drastic enhancement of light-matter interaction phenomena. We study the optical response of a one-dimensional photonic crystal slab with Kerr focusing nonlinearity in the vicinity of BICs analytically and numerically. We predict a strong nonlinear response including multistable behavior, self-tuning of BICs to the frequency of incident waves, and breaking of symmetry protected BICs. We show that all of these phenomena can be observed in silicon photonic structure at the pump power of several $\mu\text{W}/\text{cm}^2$. We also analyze the modulation instability of the obtained solutions and the effect of the finite size of the structure on the stability. Our findings have strong implications for nonlinear photonics and integrated optical circuits.

DOI: [10.1103/PhysRevB.97.224309](https://doi.org/10.1103/PhysRevB.97.224309)**I. INTRODUCTION**

Bound states in the continuum [1] (BICs) comprise a special class of localized solutions of wave equations, which have the energy lying in the continuum of the delocalized states. These states may be interpreted as resonant states with infinite quality factor, which originate due to destructive interference of several leaky modes of the system. BICs are a general feature of wave dynamics, and so may arise for quantum-mechanical particles [2–4], sound waves [5–7], water waves [8–10], and photonic structures [11–20]. The systems supporting optical BICs are usually realized as two- or one-dimensional periodic photonic structures, such as photonic crystal slabs [21] or patterned photonic wires [22,23]. The *continuum* in this case represents the states which have the tangential component of the wave vector smaller than the total wave vector of the plane wave in a surrounding medium at the same frequency. Leaky modes as well as BICs lie inside the continuum. However, leaky modes are coupled to the extended waves and therefore radiate. In contrast, BICs have no access to radiative channels due to the destructive interference so they remain localized with zero leakage and do not decay in time [see Figs. 1(c) and 1(d)]. Under the term “localized” we imply localization in the direction perpendicular to the slab interface. We need to highlight that the spectrum of the considered modes lies above the light line where only the leaky modes can exist; however, even in this case we can have localization in the Γ point. The field of the localized mode is contributed only by the near fields (closed diffraction channels) [Fig. 1(d), right panel], in contrast to leaky modes which have radiation far field [Fig. 1(d), left panel].

The bound states in the continuum in photonic crystal slabs and plasmonic lattices, being high-quality-factor resonant modes, have already found applications for sensing [24], filtering [25], and lasing [26,27]. One of the most straightforward possible applications of high-quality resonance modes such

as BICs is the enhancement of optical nonlinear effects. The nonlinear dynamics of bound states in the continuum has been explored quite recently in Fabry-Perot cavities [28] containing nonlinear impurities [29]. Moreover, nonlinear bound states in the continuum, which are conventionally referred to as embedded solitons, have been actively studied for more than a decade in nonlinear fibers [30]. Nonlinear bound states and related diffraction problems were also studied in periodic arrays of circular cylinders [31,32].

The simplest manifestation of the nonlinear dynamics in the resonant photonic structures is the multistable optical response. If a nonlinear system is pumped by an input beam the frequency of which is detuned from the linear resonant frequency, then the nonlinear frequency shift of the appropriate sign may tune the system in resonance with the pump beam which is the origin of the multistability [33]. The optical multistability (or bistability as the most simple case) has direct applications for the realization of all-optical switchers. In real structures, bistability onset is determined by the threshold pump power density, which depends on the nonlinear susceptibility of the material and the resonator quality factor. An ultra-high-quality factor of the BIC thus suggests low threshold powers for the bistability onset.

In this paper, we study the nonlinear response of a one-dimensional photonic crystal slab with Kerr-type focusing nonlinearity supporting BICs. We analyze the role of BICs in formation of bistable and tristable states, and study the modulation instability accounting for a finite size of the photonics structure. We show that the BIC supporting systems allow one to achieve strong nonlinear response without a cavity at low pump power.

II. COUPLED-MODE EQUATIONS

The structure under consideration is shown in Fig. 1(a). For the sake of simplicity, we focus only on the TE-polarized waves since the problem is reduced to the scalar form in this case. We will describe the structure in terms of effective refractive index

^{*}s.krasikov@metalab.ifmo.ru

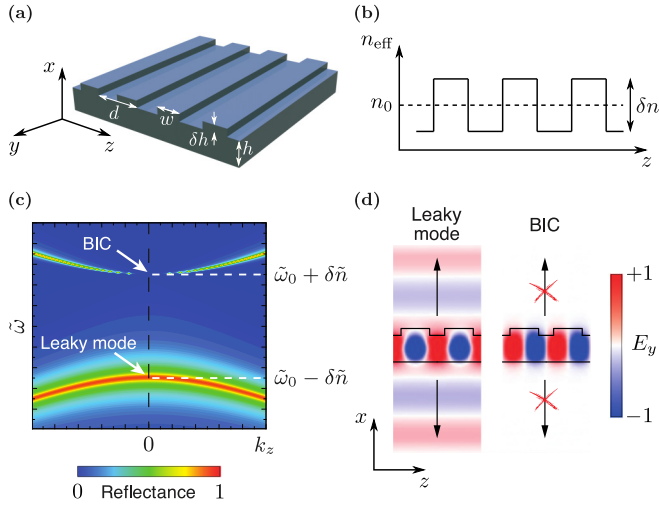


FIG. 1. (a) Schematic image of the considered system: one-dimensional photonic crystal slab. (b) Schematic representation of the periodic variation of the effective refractive index. (c) Map of the reflection coefficient vs in-plane wave vector and frequency. (d) Electric-field distribution of the leaky (symmetric) mode and bound state in the continuum (antisymmetric mode). Out of the slab the BIC is localized and its field exponentially decays away with decrement $\kappa = \sqrt{(2\pi/d)^2 - k_0^2}$, where k_0 is the normalized frequency of the BIC.

considering periodicity and nonlinearity as perturbations:

$$n(z) = n_0 + \delta n \frac{2}{\pi} \sum_{j=1}^{\infty} \frac{1}{j} \sin\left(\frac{j\pi w}{d}\right) \cos(jGz) + n_2 I. \quad (1)$$

Here n_0 is the average refractive index of the core layer in the absence of grating, δn is the modulation amplitude, $G = 2\pi/d$ is the reciprocal vector of the structure, d is the period of the lattice, w is the width of the protrusions, and $n_2 I$ is the term corresponding to the Kerr-type focusing nonlinearity. Both n_0 and δn are found from the solution of the conventional slab waveguide problem. The geometry of the waveguide is chosen such that the reciprocal vector G is close to the wave vector of the effective waveguide mode. Thus, the normally incident radiation resonantly excites forward and backward propagating waveguide modes, which are coupled via backscattering. Then we exploit the coupled-mode theory in the simplest form of two-mode approximation [34–36]. The electric field can be written as

$$E(z, t) = [E_+(z, t)e^{i\beta z} + E_-(z, t)e^{-i\beta z}]e^{-i\omega_0 t} + \text{c.c.} \quad (2)$$

Here E_{\pm} are the amplitudes of the forward and backward propagating modes with the wave vector β . Implementation of the slow-varying approximation allows one to neglect the second derivatives in the wave equation. The terms proportional to δn^2 , $(n_2 I)^2$, and $\delta n \times n_2 I$ are omitted. Moreover, we assume $\omega_0 = ck_0 = \beta c/n_0$ and use $\beta = G = 2\pi/d$ omitting all terms which have spatial dependence other than $e^{\pm i\beta z}$. With these assumptions, the wave equation can be transformed to a pair of dimensionless coupled-mode equations (see Supplemental Material [37]):

$$\frac{\partial \tilde{E}_{\pm}}{\partial \tilde{t}} = \mp \frac{\partial \tilde{E}_{\pm}}{\partial \tilde{z}} + i\delta \tilde{n} \tilde{E}_{\mp} + i\tilde{E}_{\pm} (|\tilde{E}_{\pm}|^2 + 2|\tilde{E}_{\mp}|^2). \quad (3)$$

Here we use the following normalized parameters:

$$\tilde{z} = \beta z, \quad \tilde{E}_{\pm} = E_{\pm}(n_2/n_0)^{1/2}, \\ \tilde{t} = \omega t, \quad \delta \tilde{n} = \delta n \sin(2\pi w/d)/(2\pi n_0).$$

Further, we will consider only spatially uniform solutions, and thus drop the spatial derivatives. These equations, however, should be supplemented though with the pump and decay terms. This procedure can be done in a way similar to one presented in Ref. [38]. At first, we introduce the vector of the resonant mode components $\mathbf{E} = (\tilde{E}_+, \tilde{E}_-)^T$. Moreover, we introduce the vectors of incoming and outgoing fields \mathbf{S}_+ and \mathbf{S}_- . We assume that the incoming radiation is normal to the interface impinging either from the top or from the bottom interface. The energy can leave the system also only normally to the interface from top or bottom. Thus, both \mathbf{S}_+ and \mathbf{S}_- are vectors with size 2 such that $\mathbf{S}_+ = (S_{++}, S_{+-})^T$ and $\mathbf{S}_- = (S_{-+}, S_{--})^T$, where the second indices correspond to the energy flux which goes through the top (+) or the bottom (−) interface. The resulting set of equations can be written as

$$\frac{\partial \tilde{E}_p}{\partial \tilde{t}} = i\delta \tilde{n} \hat{\sigma}_{x,pq} \tilde{E}_j + iT_{pqkl} \tilde{E}_q \tilde{E}_k^* \tilde{E}_l - \hat{\Gamma}_{pq} \tilde{E}_q + \hat{D}_{pq}^T S_{+,q}, \quad (4)$$

$$\frac{\partial S_{-,p}}{\partial \tilde{t}} = \hat{C}_{pq} S_{+,q} + \hat{D}_{pq} \tilde{E}_q. \quad (5)$$

Here, $p, q, k, l = \{+, -\}$; $\hat{\sigma}_x$ is the Pauli matrix; $T_{pqkl} = \delta_{pq} \delta_{kl} (2 - \delta_{pk})$ is the tensor governing the structure of the nonlinear response; $\hat{C} = r_{\text{slab}} \hat{I} + t_{\text{slab}} \hat{\sigma}_x$ is the matrix representing the nonresonant reflection and transmission from the slab (r_{slab} , t_{slab} are the Fresnel coefficients for the effective uniform slab); and $\hat{\Gamma} \hat{D}$ are unknown matrices responsible for the decay of the resonant modes and their coupling with incoming and outgoing waves, respectively. In Ref. [38], certain relations between $\hat{\Gamma}$, \hat{D} , and \hat{C} were derived from the energy conservation and time-reversal invariance condition. Namely, it was shown that

$$\hat{D}^\dagger \hat{D} = 2\hat{\Gamma}, \quad (6)$$

$$\hat{C} \hat{D}^* = -\hat{D}. \quad (7)$$

These relations are met even for nonlinear system, since nonlinearity is conservative and does not break the time-reversal symmetry. Because of the symmetry of the problem we seek \hat{D} and $\hat{\Gamma}$ in the form

$$\hat{D} = e^{i\phi_0} \begin{pmatrix} \sqrt{\tilde{\gamma}} & \sqrt{\tilde{\gamma}} \\ \sqrt{\tilde{\gamma}} & \sqrt{\tilde{\gamma}} \end{pmatrix}, \quad \hat{\Gamma} = \begin{pmatrix} \tilde{\gamma} & \tilde{\gamma} \\ \tilde{\gamma} & \tilde{\gamma} \end{pmatrix}. \quad (8)$$

The constant $\tilde{\gamma} = \gamma/(2\beta^2)$ can be estimated from the consideration that the coupling efficiency is proportional to the refractive index contrast, namely, $\gamma \approx k_0^2 \delta n^2$. This approximate value comes from the perturbation theory, in which the scattering rate from one mode to another is proportional to the overlap integral $\langle \psi_1 | V | \psi_2 \rangle$, where $V(x) = k_0^2 \delta n^2 \cos(\pi x/d)$. The phase ϕ_0 is found from the condition (7) and yields $\phi_0 = -1/2i \log(-r_{\text{slab}} - t_{\text{slab}})$. For the case of a thin waveguide it can be approximated by $\phi_0 \approx (n_0 k_0 h + \pi)/2$, where h is the thickness of the waveguide. The set of equations is then

rewritten as

$$\begin{aligned} \frac{\partial \tilde{E}_{\pm}}{\partial \tilde{t}} &= i\delta\tilde{n}\tilde{E}_{\mp} - \tilde{\gamma}(\tilde{E}_{+} + \tilde{E}_{-}) \\ &+ i\tilde{E}_{\pm}(|\tilde{E}_{\pm}|^2 + 2|\tilde{E}_{\mp}|^2) + \sqrt{\tilde{\gamma}\tilde{I}_p}e^{i\phi_0 - i\delta\tilde{\omega}\tilde{t}}. \end{aligned} \quad (9)$$

Here $\tilde{I}_p = n_2 E_p^2/2$ and $\delta\tilde{\omega} = \delta\omega/\omega$ is the detuning between the pump beam and $\tilde{\omega}_0 = \omega_0/\omega$. The above equations can be rewritten in terms of symmetric (leaky) and antisymmetric (BIC) modes, represented by $\tilde{E}_s = \tilde{E}_{+} + \tilde{E}_{-}$ and $\tilde{E}_a = \tilde{E}_{+} - \tilde{E}_{-}$, respectively:

$$\frac{\partial \tilde{E}_a}{\partial \tilde{t}} = (-i\delta\tilde{n} + 3iK)\tilde{E}_a - i\tilde{E}_s M, \quad (10)$$

$$\frac{\partial \tilde{E}_s}{\partial \tilde{t}} = (i\delta\tilde{n} - 2\tilde{\gamma} + 3iK)\tilde{E}_s - i\tilde{E}_a M + 2\sqrt{\tilde{\gamma}\tilde{I}_p}e^{i\phi_0 - i\delta\tilde{\omega}\tilde{t}} \quad (11)$$

where $K = \frac{1}{4}(|\tilde{E}_s|^2 + |\tilde{E}_a|^2)$ and $M = \frac{1}{4}(\tilde{E}_a\tilde{E}_s^* + \tilde{E}_s\tilde{E}_a^*)$. This pair of the equations clearly shows the absence of radiation losses for the antisymmetric mode, because $\tilde{\gamma}$ is not explicitly included in Eq. (10). For the same reason we cannot pump the BIC from the far field and its excitation is possible only because of the nonlinear coupling with a bright (symmetric) mode.

III. SELF-TUNING OF THE BIC AND SYMMETRY BREAKING

In the absence of pumping and nonlinearity, the system of Eqs. (9) has symmetric and antisymmetric solutions:

$$\tilde{\omega} = \delta\tilde{n}, \quad \tilde{E}_{+} = -\tilde{E}_{-}, \quad (12)$$

$$\tilde{\omega} = -\delta\tilde{n} - 2i\tilde{\gamma}, \quad \tilde{E}_{+} = \tilde{E}_{-}. \quad (13)$$

The antisymmetric solution has no radiation losses and corresponds to the symmetry protected BIC whereas the symmetric solution corresponds to leaky modes [see Figs. 1(b) and 1(c)]. In the nonlinear case, the amplitude of the BIC depends on the frequency:

$$|\tilde{E}_{\pm}| = \sqrt{\frac{1}{3}(\delta\tilde{n} - \tilde{\omega})}. \quad (14)$$

Therefore, in the case of Kerr-type focusing nonlinearity, the BIC exists at all the frequencies smaller than the frequency of the linear BIC ($\tilde{\omega} < \delta\tilde{n}$). This is the manifestation of the *self-tuning of the BIC*. If we pump the sufficient energy density in the system, namely, $W = d^{-1} \int |E(z)|^2 dz = (1/3)(\delta\tilde{n} - \tilde{\omega})$, then the resonant frequency is tuned such that the BIC coincides with pump frequency. This can be regarded as a way to excite the BIC: we pump the system with nonresonant radiation, and the system adjusts itself due to the nonlinearity to form a BIC. This type of behavior of nonlinear BICs has been previously discussed in Refs. [39,40] for the nonlinear Fabry-Perot resonator and nonlinear impurity model.

We then look for the solutions of the inhomogeneous set of equations in the form $E_{\pm} = -ia_{\pm}e^{i\phi_0 - i\delta\omega t}$. The resulting set of nonlinear algebraic equations has three classes of solutions. The first one is the symmetric solution $a_{+} = a_{-} = a_s$. This

class of solutions generates a standard S-shaped bistability curve and will be treated numerically in Sec. IV. The second class is that of asymmetric solutions, which have the form $a_{\pm} = a_0 e^{i\phi_{\pm}}$, where a_0 does not depend on \tilde{I}_p . These solutions are written as

$$a_0 = \sqrt{\frac{1}{3}(\delta\tilde{n} - \delta\tilde{\omega})}, \quad (15)$$

$$\tan\left(\frac{\phi_{+} + \phi_{-}}{2}\right) = -\tilde{\gamma}/\delta\tilde{n}, \quad (16)$$

$$\cos\left(\frac{\phi_{+} - \phi_{-}}{2}\right) = \frac{\sqrt{\tilde{\gamma}\tilde{I}_p}}{2a_0\sqrt{\tilde{\gamma}^2 + \delta\tilde{n}^2}}. \quad (17)$$

It can be seen that as I_p approaches zero the solution approaches the fully antisymmetric solution $\phi_{+} - \phi_{-} = \pi$. Moreover, as $\tilde{I}_p = \frac{4}{3\tilde{\gamma}}(\delta\tilde{n} - \delta\tilde{\omega})(\tilde{\gamma}^2 + \delta\tilde{n}^2)$, the solution becomes fully symmetric. A similar type of solutions, for which the pump power affects only the phase shift, has been explored in Ref. [41] for the case of the nonlinear impurity model. It was termed *Josephson-like current*, since, like in Josephson effect, the sine of the phase difference is proportional to the current (pump intensity in our case). Note, that these solutions may be stable in finite-size systems as we will show, in Sec. V. Moreover, systems of coupled dissimilar waveguides support the analogous asymmetric nonlinear modes which are also stable under the presence of gain and loss [42]. Finally, there is a class of asymmetric solutions for which $|a_{+}| \neq |a_{-}|$ and $\phi_{+} = \pi + \phi_{-}$. These solutions will be treated numerically in the next section.

IV. NUMERICAL SIMULATION

In this section, we carry out the numerical study of coupled-mode equations (9) and the reflection coefficient, which can be written as

$$R = \left| r_{\text{slab}} + \sqrt{\frac{\tilde{\gamma}}{\tilde{I}_p}}\tilde{E}_{+}e^{i\phi_0} + \sqrt{\frac{\tilde{\gamma}}{\tilde{I}_p}}\tilde{E}_{-}e^{i\phi_0} \right|^2. \quad (18)$$

For the numerical calculations we use the following set of parameters: we considered a silicon slab waveguide in vacuum ($n_0 = 3.48$, $n_2 = 3 \times 10^{-18}$ m²/W [43,44]). The depth of the etched grating was chosen to be 10 nm while the thickness of the core layer without grating is $h = 100$ nm; the refractive index modulation amplitude in this case is $\delta n \approx 0.0316$. The lattice period d was chosen in such a way that $\beta = 2\pi/d$ at wavelength $\lambda = 1$ μm . Width of the protrusions is chosen to be $w = d/4$. We have also added the material losses to the system by introducing additional diagonal loss term $\delta\gamma = 0.25\gamma$ to matrix $\hat{\Gamma}$. The results of the numerical modeling are shown in Fig. 2.

Figure 2(a) shows the phase diagram depending on the pump detuning and intensity. The four numbers labeling different phases correspond to the number of stationary solutions, number of stable solutions, number of symmetric solutions, and number of stable symmetric solutions, respectively. Here, stability was checked with respect to homogeneous perturbations. It has been anticipated that nonlinear BICs can be destroyed by the modulation instability. It has been even suggested to exploit

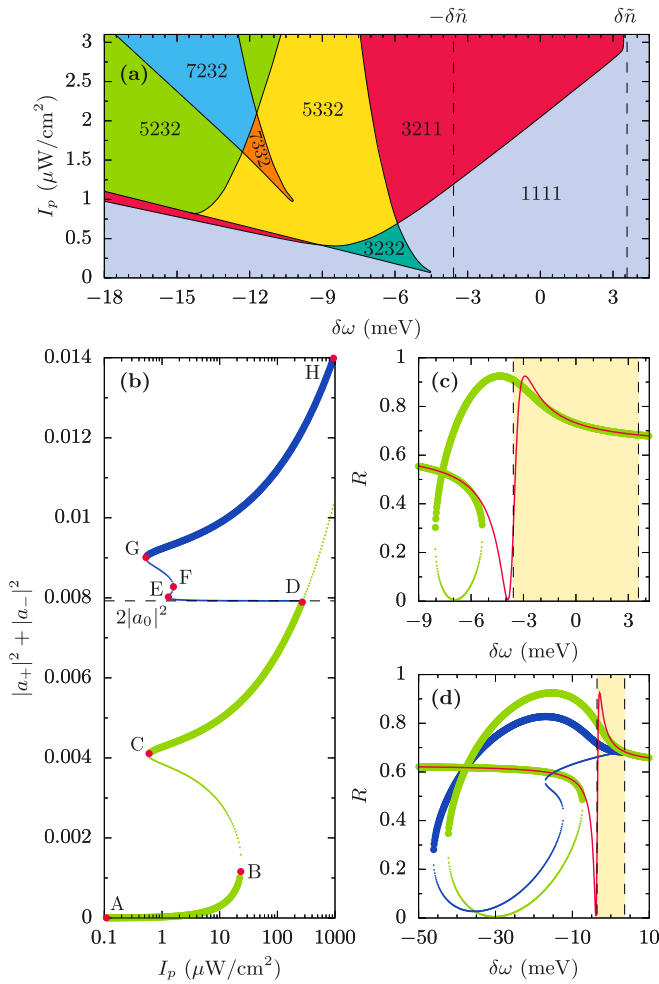


FIG. 2. Graphical representation of the solutions of coupled-mode equations (9). The four-digit numerical indices $abcd$ in panel (a) have the following meaning: a shows the total number of solutions, b denotes how many of them are stable, c is the number of symmetric solutions, and d is the number of stable symmetric solutions. The total field as a function of pump intensity is shown in panel (b) where $\delta\omega = -11.16$ meV. Note that the horizontal axis there has logarithmic scale. Labeled points are used to distinguish between different branches of solutions. (c, d) Reflection coefficient of the structure with respect to detuning $\delta\omega$ at $I_p \sim 0.34$ (c) and $3 \mu\text{W}/\text{cm}^2$ (d). All other parameters are the same for all panels and are given in the main text. In panels (c) and (d), green dots correspond to symmetric solutions, blue dots correspond to asymmetric solutions, and red lines indicate the linear solutions. The stable (unstable) solutions are shown by thick (tiny) dots. The dashed line in panel (b) corresponds to antisymmetric solutions $2|a_0|^2$. The shaded area in panels (c) and (d) indicates the region $-\delta\tilde{n} < \delta\tilde{\omega} < \delta\tilde{n}$.

the instability to generate the frequency combs using BICs [45]. It can be seen that for the large positive detunings $\delta\omega > \delta n$ the system supports a single symmetric stable solution. In the region $-\delta n < \delta\omega < \delta n$ and large enough intensity, another phase exists where two additional asymmetric solutions emerge, one of which is stable. Therefore, the nonlinearity could result in *breaking of the symmetry protected BIC* and its transformation into symmetric solution with radiation losses.

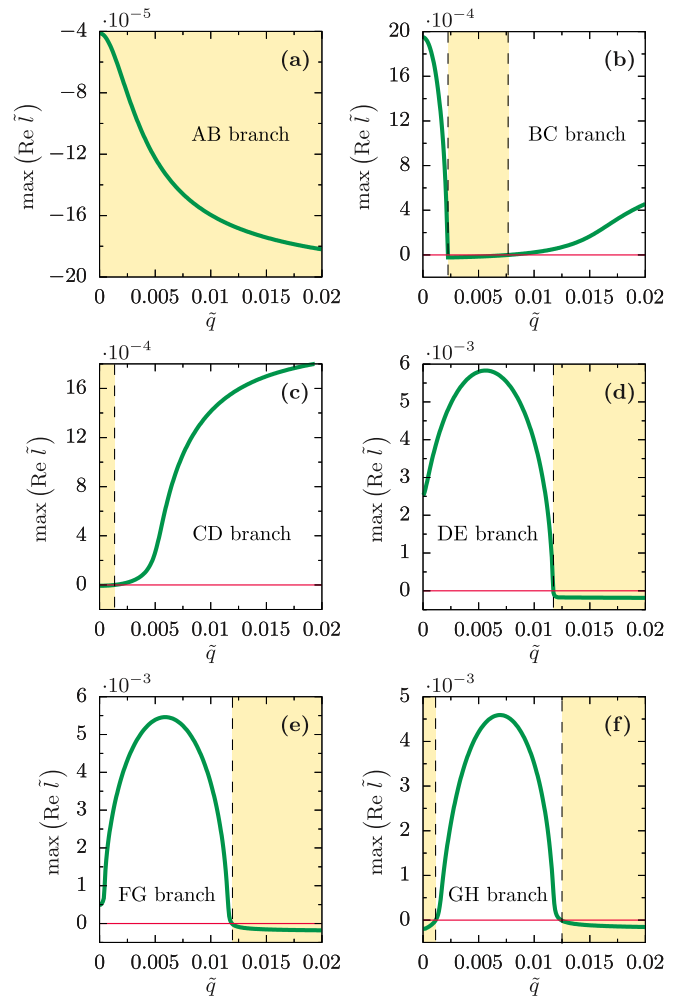


FIG. 3. Stability analysis of the solution presented in Fig. 2(b) for which $q = 0$, i.e., the system is infinitely large. Therefore, Fig. 3 represents how decrease of the system size (increase of q) affects stability of modes. Text in the panels corresponds to solutions shown in Fig. 2(b). The shaded area indicates stable solutions. For each plot $I_p \approx 1.5 \mu\text{W}/\text{m}^2$ and $\delta\omega = -11.16$ meV. All other parameters are given in the main text.

The situation complicates drastically as detuning becomes less than $-\delta n$. Namely, already at moderate pumping intensities, a multistable behavior is observed with two symmetric and one asymmetric stable solution. We plot the dependence of the mode intensity on the pumping power for $\delta\omega = -11.16$ meV in Fig. 2(b). The symmetric solutions are shown in green, and they exhibit conventional bistable behavior. At the same time, we observe the additional nonsymmetry branch shown in blue. Remarkably, in the absence of material losses ($\delta\gamma = 0$) the blue branch starts from the zero intensity manifesting the fully antisymmetric BIC. It then splits into the horizontal branch which connects it with the symmetric solution and the branch of asymmetric solutions, which exhibits S-shape behavior.

The asymmetric solutions generate the energy flow in the plane of the waveguide S_z , which is proportional to $|a_+|^2 - |a_-|^2$. Since the asymmetric solutions appear in pairs equivalent up to interchange of a_+ and a_- , the specific current direction is defined by the initial conditions. The spectra of the

reflection coefficient at different pump intensities are shown in Figs. 2(c) and 2(d) and are compared with the linear reflection coefficient (thin red line).

V. MODULATION INSTABILITY

As the next step, we analyze stability of the obtained solutions with respect to the longitudinal perturbations. For that we write the electric field in the form

$$\tilde{E}_{\pm}(\tilde{z}, \tilde{t}) = (a_{\pm} + \epsilon f_{\pm} e^{i\tilde{q}\tilde{z}} e^{i\tilde{t}} + \epsilon g_{\pm} e^{-i\tilde{q}\tilde{z}} e^{i\tilde{t}}) e^{-i\delta\tilde{\omega}\tilde{t}}, \quad (19)$$

where ϵ is the amplitude of the small perturbation; \tilde{q} is the wave vector of the perturbation, which is a parameter; and \tilde{t} is the complex eigenfrequency. We substitute the expression for the electric field to the initial differential equations and linearize them with respect to ϵ . The solution of the resulting eigenvalue problem for \tilde{t} gives the spectrum of the linear perturbations. If at least one of the eigenvalues has positive real part, then our initial solution is unstable. Figure 3 shows the spectra of the linear perturbations with largest real part of \tilde{t} for different classes of stationary solutions. The stability with respect to homogeneous perturbations labeled in Fig. 2 corresponds to the case of $\tilde{q} = 0$. We can see that while the lower stable branch of the symmetric solution is stable for all possible \tilde{q} [Fig. 3(a)] the upper branch is unstable to the perturbations with any finite \tilde{q} larger than some critical \tilde{q}_{crit} [Fig. 3(b)]. It has been shown previously for a similar system that the instability of the upper symmetric branch leads to soliton formation [46]. At the same time, we can see that all of the asymmetric

solutions are stable with respect to perturbations with wave vectors larger than some finite critical value \tilde{q}_{max} , as can be seen in Figs. 3(d)–3(f). This has interesting consequences for the stability conditions in finite structures. Namely, since only perturbations which have wavelength smaller than the system size may exist, the perturbations with $\tilde{q} < 1/N$ (where N is the number of periods) will decay. Thus, if the system size is less than \tilde{q}_{max} , it will be linearly stable with respect to longitudinal perturbation. Therefore, a finite size of the structure could stabilize the solutions, which are unstable in the infinite system.

VI. CONCLUSION

To conclude, we have demonstrated the existence of the nonlinear BIC in a simple structure periodically corrugated silicon waveguide. We have shown how the existence of the BIC leads to the emergence of multistable behavior in the structure at moderate pump intensities. Moreover, it has been shown that finite system size may stabilize the solutions, which are unstable in the infinite system. The moderate level of pump intensities required for the optical switching in the structures supporting BIC states opens avenues for the realization of all-optical switchers exploiting bound states in the continuum.

ACKNOWLEDGMENT

This paper is supported by the Russian Science Foundation (Grant No. 17-12-01581).

-
- [1] C. W. Hsu, B. Zhen, A. D. Stone, J. D. Joannopoulos, and M. Soljačić, *Nat. Rev. Mater.* **1**, 16048 (2016).
 - [2] J. von Neumann and E. P. Wigner, in *The Collected Works of Eugene Paul Wigner* (Springer, Berlin, Heidelberg, 1993), pp. 291–293.
 - [3] F. H. Stillinger and D. R. Herrick, *Phys. Rev. A* **11**, 446 (1975).
 - [4] F. Capasso, C. Sirtori, J. Faist, D. L. Sivco, S.-N. G. Chu, and A. Y. Cho, *Nature (London)* **358**, 565 (1992).
 - [5] R. Parker, *J. Sound Vib.* **5**, 330 (1967).
 - [6] W. Koch, *J. Sound Vib.* **88**, 233 (1983).
 - [7] D. Evans, M. Levitin, and D. Vassiliev, *J. Fluid Mech.* **261**, 21 (1994).
 - [8] F. Ursell, *Math. Proc. Cambridge Philos. Soc.* **47**, 347 (1951).
 - [9] C. Retzler, *Appl. Ocean Res.* **23**, 249 (2001).
 - [10] P. Cobelli, V. Pagneux, A. Maurel, and P. Petitjeans, *J. Fluid Mech.* **666**, 445 (2011).
 - [11] A.-S. Bonnet-Bendhia and F. Starling, *Math. Methods Appl. Sci.* **17**, 305 (1994).
 - [12] P. Paddon and J. F. Young, *Phys. Rev. B* **61**, 2090 (2000).
 - [13] A. L. Yablonskii, E. A. Muljarov, N. A. Gippius, S. G. Tikhodeev, T. Fujita, and T. Ishihara, *J. Phys. Soc. Jpn.* **70**, 1137 (2001).
 - [14] S. G. Tikhodeev, N. A. Gippius, A. Christ, T. Zentgraf, J. Kuhl, and H. Giessen, *Phys. Status Solidi C* **2**, 795 (2005).
 - [15] S. G. Tikhodeev, A. L. Yablonskii, E. A. Muljarov, N. A. Gippius, and T. Ishihara, *Phys. Rev. B* **66**, 045102 (2002).
 - [16] J. Lee, B. Zhen, S.-L. Chua, W. Qiu, J. D. Joannopoulos, M. Soljačić, and O. Shapira, *Phys. Rev. Lett.* **109**, 067401 (2012).
 - [17] Z. F. Sadrieva, I. S. Sinev, K. L. Koshelev, A. Samusev, I. V. Iorsh, O. Takayama, R. Malureanu, A. A. Bogdanov, and A. V. Lavrinenko, *ACS Photon.* **4**, 723 (2017).
 - [18] H. M. Doeleman, F. Monticone, W. Hollander, A. Alù, and A. F. Koenderink, *Nat. Photon.* **1** (2018), doi:10.1038/s41566-018-0177-5.
 - [19] A. A. Bogdanov, K. L. Koshelev, P. V. Kapitanova, M. V. Rybin, S. A. Gladyshev, Z. F. Sadrieva, and M. F. Limonov, *arXiv:1805.09265* (2018).
 - [20] M. V. Rybin, K. L. Koshelev, Z. F. Sadrieva, K. B. Samusev, A. A. Bogdanov, M. F. Limonov, and Y. S. Kivshar, *Phys. Rev. Lett.* **119**, 243901 (2017).
 - [21] C. W. Hsu, B. Zhen, J. Lee, S.-L. Chua, S. G. Johnson, J. D. Joannopoulos, and M. Soljačić, *Nature (London)* **499**, 188 (2013).
 - [22] E. N. Bulgakov and A. F. Sadreev, *Phys. Rev. A* **96**, 013841 (2017).
 - [23] M. A. Belyakov, M. A. Balezin, Z. F. Sadrieva, P. V. Kapitanova, E. A. Nenasheva, A. F. Sadreev, and A. A. Bogdanov, *arXiv:1806.01932* (2018).
 - [24] A. A. Yanik, A. E. Cetin, M. Huang, A. Artar, S. H. Mousavi, A. Khanikaev, J. H. Connor, G. Shvets, and H. Altug, *Proc. Natl. Acad. Sci. USA* **108**, 11784 (2011).
 - [25] J. M. Foley, S. M. Young, and J. D. Phillips, *Phys. Rev. B* **89**, 165111 (2014).
 - [26] K. Hirose, Y. Liang, Y. Kurosaka, A. Watanabe, T. Sugiyama, and S. Noda, *Nat. Photon.* **8**, 406 (2014).

- [27] A. Kodigala, T. Lepetit, Q. Gu, B. Bahari, Y. Fainman, and B. Kanté, *Nature (London)* **541**, 196 (2017).
- [28] E. N. Bulgakov and A. F. Sadreev, *Phys. Rev. B* **81**, 115128 (2010).
- [29] E. N. Bulgakov and A. F. Sadreev, *Phys. Rev. B* **80**, 115308 (2009).
- [30] J. Yang, B. Malomed, D. Kaup, and A. Champneys, *Math. Comput. Simul.* **56**, 585 (2001).
- [31] L. Yuan and Y. Y. Lu, *Opt. Express* **23**, 20636 (2015).
- [32] L. Yuan and Y. Y. Lu, *Phys. Rev. A* **94**, 013852 (2016).
- [33] G. P. Agrawal and H. J. Carmichael, *Phys. Rev. A* **19**, 2074 (1979).
- [34] H. Kogelnik, in *Integrated Optics* (Springer, Berlin, 1975), Chap. 2, pp. 13–81.
- [35] J. E. Sipe, L. Poladian, and C. M. de Sterke, *J. Opt. Soc. Am. A* **11**, 1307 (1994).
- [36] H. Kogelnik and C. V. Shank, *Appl. Phys. Lett.* **18**, 152 (1971).
- [37] See Supplemental Material at <http://link.aps.org/supplemental/10.1103/PhysRevB.97.224309> for the details of derivation.
- [38] Wonjoo Suh, Zheng Wang, and Shanhui Fan, *IEEE J. Quantum Electron.* **40**, 1511 (2004).
- [39] E. Bulgakov, K. Pichugin, and A. Sadreev, *Opt. Express* **23**, 22520 (2015).
- [40] K. Pichugin and A. Sadreev, *Phys. Lett. A* **380**, 3570 (2016).
- [41] E. Bulgakov, K. Pichugin, and A. Sadreev, *J. Phys.: Condens. Matter* **23**, 065304 (2011).
- [42] Y. Kominis, T. Bountis, and S. Flach, *Sci. Rep.* **6**, 33699 (2016).
- [43] Q. Lin, J. Zhang, G. Piredda, R. W. Boyd, P. M. Fauchet, and G. P. Agrawal, *Appl. Phys. Lett.* **91**, 021111 (2007).
- [44] A. D. Bristow, N. Rotenberg, and H. M. Van Driel, *Appl. Phys. Lett.* **90**, 191104 (2007).
- [45] K. N. Pichugin and A. F. Sadreev, *J. Opt. Soc. Am. B* **32**, 1630 (2015).
- [46] A. Yulin, D. V. Skryabin, and P. S. J. Russell, *Opt. Express* **13**, 3529 (2005).